

Lithography Simulation in Semiconductor Manufacturing

Chris A. Mack

KLA-Tencor, FINLE Division

8834 N. Capital of Texas Highway, Suite 301, Austin, TX 78759 USA

Phone: (512) 327-3781; Fax: (512) 327-1510; e-mail: chris.a.mack@kla-tencor.com

ABSTRACT

In the 30 years since lithography modeling was first introduced, optical lithography simulation has progressed from a curiosity, to a research and development tool, and finally to a manufacturing tool. While much has been published on new developments in lithography simulators and their use in advanced lithography development, less is published on how simulators have been used and are soon to be used in semiconductor manufacturing flows. This review paper will describe the most popular and useful examples today for lithography simulators in a manufacturing environment.

Keywords: Lithography Simulation, PROLITH, semiconductor manufacturing

1. INTRODUCTION

In the 30 years since optical lithography modeling was first introduced to the semiconductor industry, it has gone from a research curiosity to an indispensable tool for research, development and manufacturing. There are numerous examples of how modeling has had a dramatic impact on the evolution of lithography technology, and many more ways in which it has subtly, but undeniably, influenced the daily routines of lithography professionals. There are four major uses for lithography simulation: 1) as a research tool, performing experiments that would be difficult or impossible to do any other way, 2) as a development tool, quickly evaluating options, optimizing processes, or saving time and money by reducing the number of experiments in the fab, 3) as a manufacturing tool, for troubleshooting process problems and determining optimum process settings, and 4) as a learning tool, to help provide a fundamental understanding of all aspects of the lithography process. These four applications of lithography simulation are not distinct – there is much overlap among these basic categories.

A. Research Tool

Since the initial introduction of lithography simulation in 1975, modeling has had a major impact on research efforts in lithography. Here are some early examples of how modeling has been used in research.

Modeling was used to suggest the use of dyed photoresist in the reduction of standing waves [1]. Experimental investigation into dyed resists didn't begin until 10 years later [2,3]. After phase-shifting masks were first introduced [4], modeling has proven to be indispensable in their study. Levenson used modeling extensively to understand the effects of phase masks [5]. One of the earliest studies of phase-shifting masks used modeling to calculate images for Levenson's original alternating phase mask, then showed how phase masks increased defect printability [6]. The same study used modeling to introduce the

concept of the outrigger (or assist slot) phase mask. Since these early studies, modeling results have been presented in nearly every paper published on phase-shifting masks. Off-axis illumination was first introduced as a technique for improving resolution and depth of focus based on modeling studies [7]. Since then, this technique has received widespread attention and has been the focus of many more simulation and experimental efforts. Using modeling, the advantages of having a variable numerical aperture, variable partial coherence stepper were discussed [7,8]. Since then, all major stepper vendors have offered variable NA, variable coherence systems. Modeling remains a critical tool for optimizing the settings of these flexible new machines. The use of pupil filters to enhance some aspects of lithographic performance have, to date, only been studied theoretically using lithographic models [9]. If such studies prove the usefulness of pupil filters, experimental investigations may also be conducted.

Modeling has been used in photoresist studies to understand the depth of focus loss when printing contacts in negative resists [10], the reason for artificially high values of resist contrast when surface inhibition is present [11], the potential for exposure optimization to maximize process latitude [12,13], and the role of diffusion in chemically amplified resists [14]. Lithographic models are now standard tools for photoresist design and evaluation. Modeling has always been used as a tool for quantifying optical proximity effects and for defining algorithms for geometry dependent mask biasing [15,16]. Most people would consider modeling to be a required element of any optical proximity correction scheme. Defect printability has always been a difficult problem to understand. The printability of a defect depends considerably on the imaging system and resist used, as well as the position of the defect relative to other patterns on the mask and the size and transmission properties of the defect. Modeling has proven itself a valuable and accurate tool for predicting the printability of defects [17,18]. Modeling has also been used to understand metrology of lithographic structures [19-22] and continues to find new application in virtually every aspect of lithographic research. In fact, modeling has proven an indispensable tool for predicting future lithographic performance and evaluating the theoretical capabilities and limitations of extensions for optical lithography far into the future.

One of the primary reasons that lithography modeling has become such a standard tool for research activities is the ability to simulate such a wide range of lithographic conditions. While laboratory experiments are limited to the equipment and materials on hand (a particular wavelength and numerical aperture of the stepper, a given photoresist), simulation gives an almost infinite array of possible conditions. From high numerical apertures to low wavelengths, hypothetical resists to arbitrary mask structures, simulation offers the ability to run “experiments” on steppers that you do not own with photoresists that have yet to be made. How else can one explore the shadowy boundary between the possible and the impossible?

B. Process Development Tool

Lithography modeling has also proven to be an invaluable tool for the development of new lithographic processes or equipment. Some of the more common uses include the optimization of dye loadings in photoresist [23,24], simulation of substrate reflectivity [25,26], the applicability and optimization of top and bottom antireflection coatings [27,28], and simulation of the effect of bandwidth on swing curve amplitude [29,30]. In addition, simulation has been used to help understand the use of thick resists for thin film head manufacture [31] as well as other non-semiconductor applications. Modeling is used extensively by makers of photoresist to evaluate new formulations [32,33] and to determine adequate measures of photoresist performance for quality control purposes [34]. Resist users often employ modeling as an aid for new resist evaluations. On the exposure tool side, modeling has become an indispensable part of the optimization of the numerical aperture and partial coherence of a stepper [35-37] and in the understanding of the print bias between dense and isolated lines [38]. The use of optical proximity

correction software requires rules on how to perform the corrections, which are often generated with the help of lithography simulation [39].

As a development tool, lithography simulation excels due to its speed and cost-effectiveness. Process development usually involves running numerous experiments to determine optimum process conditions, shake out possible problems, determine sensitivity to variables, and write specification limits on the inputs and outputs of the process. These activities tend to be both time consuming and costly. Modeling offers a way to supplement laboratory experiments with simulation experiments to speed up this process and reduce costs. Considering that a single experimental run in a wafer fabrication facility can take from hours to days, the speed advantage of simulation is considerable. This allows a greater number of simulations than would be practical (or even possible) in the fab.

C. Manufacturing Tool

Although you will find less published material on the use of lithography simulation in manufacturing environments [40-42], the reason is the limited publications by people in manufacturing rather than the limited use of lithography modeling. The use of simulation in a manufacturing environment has three primary goals: to reduce the number of test or experimental wafers which must be run through the production line, to troubleshoot problems in the fab, and to aid in decision making by providing facts to support engineering judgment and intuition. Running test wafers through a manufacturing line is costly not so much due to the cost of the test, but due to the opportunity cost of not running product [43]. If simulation can reduce the time a manufacturing line is not running product even slightly, the return on investment can be significant. Simulation can also aid in the time required to bring a new process on-line and in the establishment of the base-line capability of a new process. Although not a complete list, the most common use cases for lithography simulation in a manufacturing environment are:

- Film Stack Optimization
- Process Window Prediction
- NA/ σ optimization
- OPC Verification
- CD Limited Yield, Cpk Analysis
- Troubleshooting/Root Cause Analysis

These use cases will be explored in more detail in subsequent sections of this paper.

D. Learning Tool

Although the research, development and manufacturing applications of lithography simulation presented above give ample benefits of modeling based on time, cost and capability, the underlying power of simulation is its ability to act as a learning tool. Proper application of modeling allows the user to learn efficiently and effectively. There are many reasons why this is true. First, the speed of simulation versus experimentation makes feedback much more timely. Since learning is a cycle (an idea, an experiment, a measurement, then comparison back to the original idea), faster feedback allows for more cycles of learning. Since simulation is very inexpensive, there are fewer inhibitions and more opportunities to explore ideas. And, as the research application has shown us, there are fewer physical constraints on what "experiments" can be performed. All of these factors allows the use of modeling to gain an understanding of lithography. Whether learning fundamental concepts or exploring subtle nuances, the value of improved knowledge can not be overstated. In the sections that follow, the use of lithography simulation in manufacturing will be explored in much greater detail.

2. THE USE OF LITHOGRAPHY SIMULATION IN MANUFACTURING

A. Film Stack Optimization

Film stack optimization is the most frequent use of lithography simulation in a manufacturing environment for a number of reasons. First, film stacks frequently change in the fab and, other than the bottom antireflection coating (BARC) and resist, this film stack is not controlled by the photolithography group. Thus, the lithography group must respond to these film stack changes with adjustments to the lithography process. From a lithography standpoint, the most important film stack property is the reflectivity of the substrate. Unfortunately, there is no way to measure the reflectivity of the substrate when coated with resist (substrate reflectivity in air has no meaning for this application). Thus, all BARC optimization efforts require the use of simulation. In turn, this simulation requires accurate measurement of BARC optical parameters (thickness, n , & k).

The goals of film stack optimization are to minimize standing waves in the resist, and to reduce the sensitivity of the process to film stack variations (including resist and BARC, but other layers as well). By far the most common way to accomplish all of these goals is by using an optimized bottom antireflection coating. When optimizing a litho process for reflectivity, there are three basic tasks: 1) optimize the BARC, 2) optimize the resist thickness (from a swing curve perspective), and 3) understand the sensitivity to BARC, resist, and film stack variations. For the first task, there are two classes of BARC problems:

- BARC on metal (absorbing substrate) – the goal is to reduce the reflectivity (the thickness of the metal or what's underneath doesn't matter)
- BARC on oxide (transparent substrate) – reduce the sensitive to oxide thickness variations (while also keeping reflectivity low)

There are three BARC parameters available for optimization: the thickness of the BARC, and the real and imaginary parts of its refractive index. For the simplest use case, a BARC is given and the goal is just to optimize its thickness. Figure 1 shows substrate reflectivity calculations for two different resist/BARC/substrate stacks. These reflectivity curves show a characteristic feature of a resist/BARC/substrate stack: the lowest reflectivity could be at the first minimum or at the second minimum. Etch and process integration considerations determine the range of acceptable BARC thicknesses, and thus the preference for a first minimum BARC or a second minimum BARC.

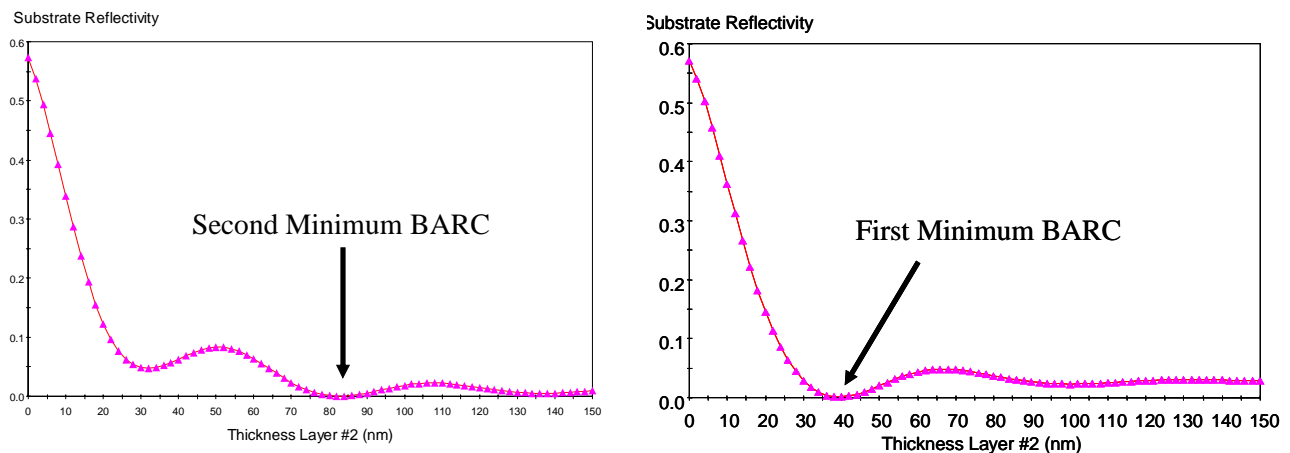


Figure 1. Typical examples of substrate reflectivity versus BARC thickness for different resist/BARC/substrate stacks.

For the case where all of the BARC properties are up for optimization, a more detailed look at the problem is required. Recapping the basic thin film reflectivity theory, the electric field reflection coefficient (the ratio of reflected to incident electric fields) at the interface between two materials is a function of the complex indices of refraction for the two layers. For normal incidence, the reflection coefficient of light traveling through layer i and striking layer j is

$$\rho_{ij} = \frac{\mathbf{n}_i - \mathbf{n}_j}{\mathbf{n}_i + \mathbf{n}_j} \quad (1)$$

where each complex index of refraction has real and imaginary parts ($\mathbf{n}_j = n_j - i\kappa_j$) and the intensity reflectivity is the square of the magnitude of this reflection coefficient. For the case of a bottom antireflection coefficient (BARC), assume the BARC (layer 2) is sandwiched between a resist (layer 1) and a very thick substrate (layer 3). The total reflectivity looking down on layer 2 includes reflections from both the top and bottom of the BARC film. The resulting reflectivity, taking into account all possible reflections, is

$$R_{total} = |\rho_{total}|^2 = \left| \frac{\rho_{12} + \rho_{23}\tau_D^2}{1 + \rho_{12}\rho_{23}\tau_D^2} \right|^2 \quad (2)$$

where the internal transmittance, τ_D , is the change in the electric field as it travels from the top to the bottom of the BARC, given by

$$\tau_D = e^{-i2\pi n_2 D / \lambda} \quad (3)$$

for a layer thickness of D .

If the role of layer 2 is to serve as an anti-reflection coating between materials 1 and 3, one obvious requirement might be to minimize the total reflectivity given by equation (2). If the light reflecting off the top of layer 2 (ρ_{12}) can cancel out the light which travels down through layer 2, reflects off layer 3, and then travels back up through layer 2 ($\rho_{23}\tau_D^2$), then the reflectivity can become exactly zero. In other words,

$$R_{total} = 0 \quad \text{when} \quad \rho_{12} + \rho_{23}\tau_D^2 = 0 \quad (4)$$

When designing a BARC material, there are only three variables that can be adjusted: the real and imaginary parts of the refractive index of the BARC, and its thickness. One classic solution to equation (4) works perfectly when the materials 1 and 3 are non-absorbing: let $\tau_D^2 = -1$ and $\rho_{12} = \rho_{23}$. This is equivalent to saying that the BARC thickness is a “quarter wave” ($D = \lambda/4n_2$), and the non-absorbing BARC has a refractive index of $n_2 = \sqrt{n_1 n_3}$. While this BARC solution is ideal for applications like antireflective coatings on lens surfaces, it is not particularly useful for common lithography substrates, which are invariably absorbing.

Will a solution to equation (4) always exist, even when the resist and substrate have complex refractive indices? Since all the terms in equation (4) are complex, zero reflectivity occurs when both the real part and the imaginary part of equation (4) are true. This can be made true but adjusting only two of the

three BARC parameters (n , κ , and D). In other words, there is not just one solution but a family of solutions to the optimum BARC problem. Expressing each reflection coefficient in terms of magnitude and phase,

$$\rho_{ij} = |\rho_{ij}| e^{i\theta_{ij}} \quad (5)$$

equation (4) can be expressed as two equalities.

$$D = \frac{\lambda}{4\pi\kappa_2} \ln \left| \frac{\rho_{23}}{\rho_{21}} \right| = \frac{\lambda}{4\pi n_2} (\theta_{23} - \theta_{21}) \quad (6)$$

Unfortunately, the seemingly simple forms of equations (4) and (6) are deceptive – solving for the unknown complex refractive index of the BARC is exceedingly messy. As a consequence, numerical solutions to equation (4) are almost always used.

Consider a common case of a BARC for 193nm exposure of resist on silicon. The ideal BARC is the family of solutions as shown in Figure 2, which gives the ideal BARC n and κ values as a function of BARC thickness. Each solution produces exactly zero reflectivity for normally incident monochromatic light.

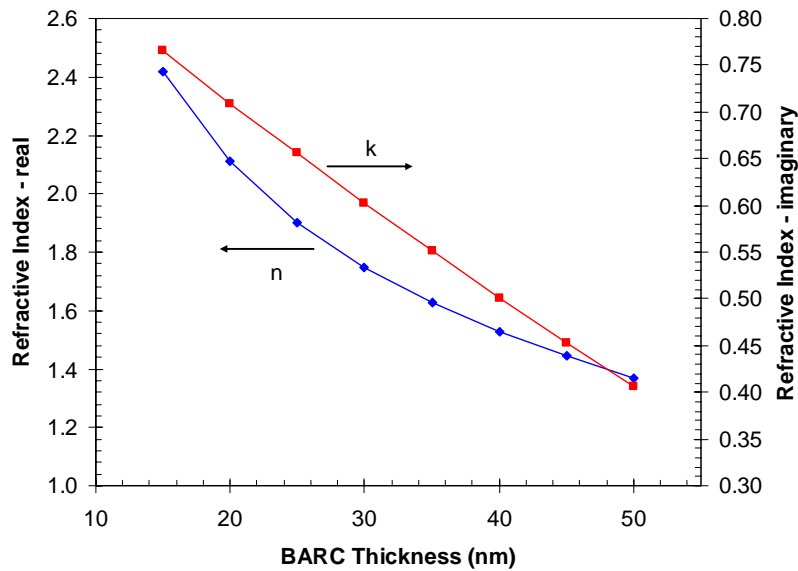


Figure 2. Optimum BARC refractive index (real and imaginary parts, n and κ) as a function of BARC thickness for normal incidence illumination (resist index = $1.7 - i0.015358$ and silicon substrate index = $0.883143 - i2.777792$) at 193nm.

Things become a bit more complicated for the more general case of light traveling at an angle with respect to the film stack normal. In lithographic terms, high numerical apertures allow large ranges of angles to pass through the lens and arrive at the wafer. Off-axis illumination of small pitch patterns produces images made of light concentrated at large angles. Small isolated features with large σ partially

coherent illumination create light reaching the wafer over a wide range of angles. And of course, low numerical apertures result in limited ranges of angles reaching the wafer.

How does non-normal incidence affect equation (2)? Each reflection coefficient ρ_{ij} is a function of the angle of light, and a function of polarization. Unpolarized light (the kind most commonly employed in lithographic tools) can be considered as the incoherent sum of two linear and orthogonal polarizations. If θ_i is the incident (and reflected) angle inside the resist and θ_t is the transmitted angle in the BARC, then the electric field reflection and transmission coefficients are given by the Fresnel formulae.

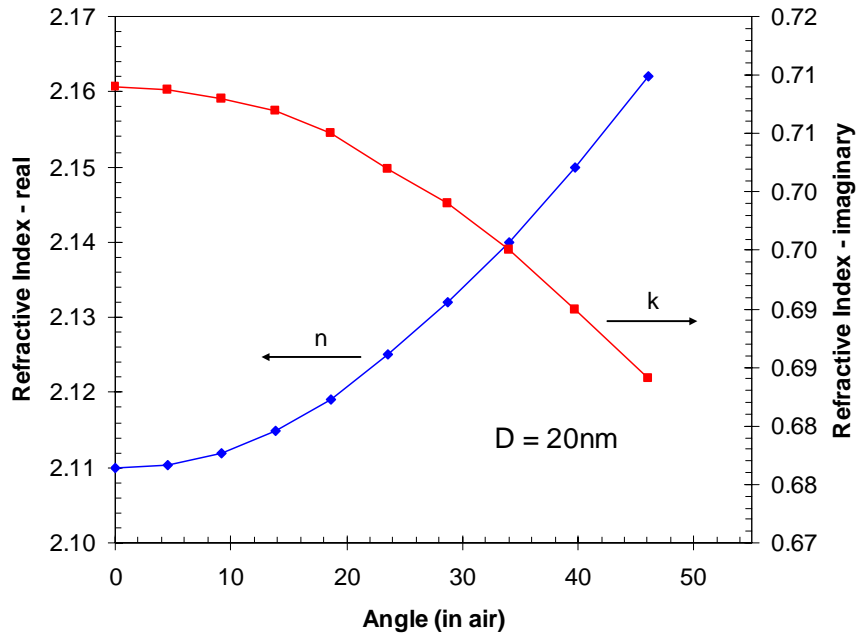
$$\rho_{12\perp} = \frac{n_1 \cos(\theta_i) - n_2 \cos(\theta_t)}{n_1 \cos(\theta_i) + n_2 \cos(\theta_t)}$$

$$\rho_{12\parallel} = \frac{n_1 \cos(\theta_t) - n_2 \cos(\theta_i)}{n_1 \cos(\theta_t) + n_2 \cos(\theta_i)} \quad (7)$$

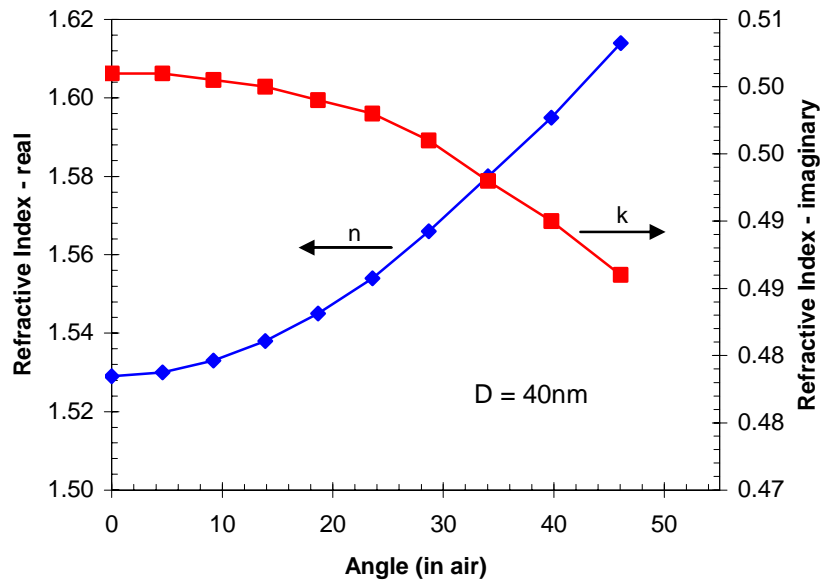
Here, \parallel represents an electric field vector which lies parallel to the plane defined by the direction of the incident light and a normal to the material interface. Other names for \parallel polarization include p polarization and TM (transverse magnetic) polarization. The polarization denoted by \perp represents an electric field vector which lies in a plane perpendicular to that defined by the direction of the incident light and a normal to the surface. Other names for \perp polarization include s polarization and TE (transverse electric) polarization. Note that for light normally incident on the resist surface, both s and p polarization result in electric fields which lie along the resist surface and the Fresnel formulae revert to the standard definition of normal incidence reflection coefficient given in equation (1). Of course, the relationship between incident and transmitted angle is given by Snell's law. The internal transmittance is also a function of angle. Equation (3) can still be used if the BARC thickness is replaced by $D \cos(\theta)$.

The requirements for zero reflectivity remain the same. Equation (4) must be satisfied for both s and p polarization. Since each equation has both real and imaginary parts, there are four constraints that must be satisfied in order to achieve exactly zero reflectivity for unpolarized illumination. However, the BARC film gives us only three degrees of freedom (n , κ , and D). In general, there can be no single BARC film that can make the reflectivity go to zero for a non-normal incident plane wave. Using PROLITH to calculate the unpolarized reflectivity (defined as the average of the individual reflectivities for s and p polarization), the best case optimum BARC parameters are given in Figure 3 as a function of incident angle (in air, before striking the resist).

Figure 4 shows the lowest possible reflectivity as a function of incident angle, using the optimum BARC parameters defined in Figure 3 for each angle. As can be seen, the best case reflectivity grows rapidly as the angle increases, and is worse for the thinner BARC film. Today's stringent CD control requirements demand reflectivities far below 1%, making BARC design difficult at high numerical apertures with extreme off-axis. One potential solution, though not pleasant from a cost and complexity perspective, is to increase the number of free variables available for optimization by using a two-layer BARC. This technique, a standard practice in antireflective coatings for lenses, would provide enough adjustable parameters to make the reflectivity go to zero at normal incidence and at one angle, thus providing low reflectivity over a wide range of angles. This approach may become necessary with the advent of immersion lithography and numerical apertures greater than 1.0.



(a)



(b)

Figure 3. Optimum BARC parameters to achieve minimum substrate reflectivity as a function of incident angle (angle defined in air, before entering the photoresist) for two different BARC thicknesses.

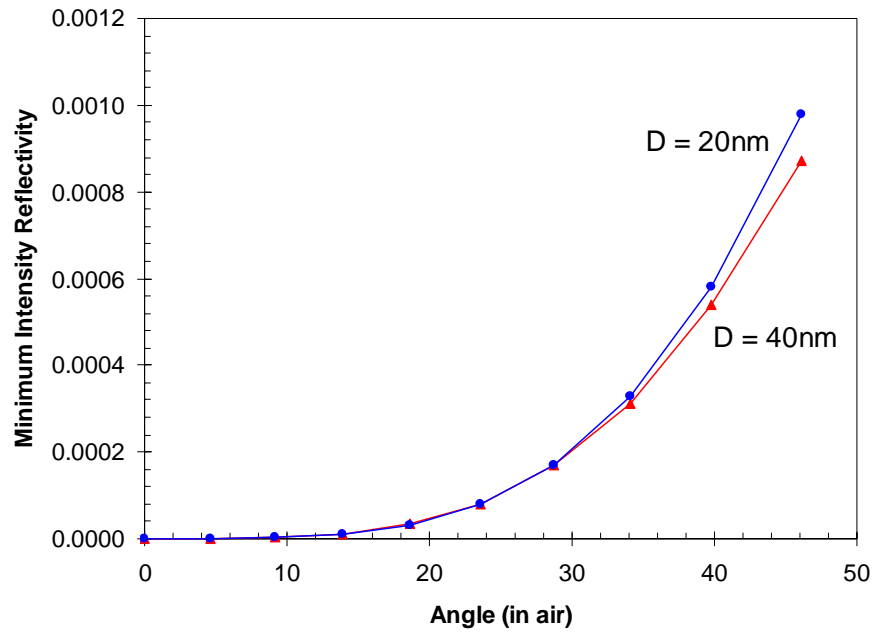


Figure 4. The best case (minimum) reflectivity (using the BARC parameters shown in Figure 2) of the substrate as a function of incident angle for 20nm and 40nm thick BARC films.

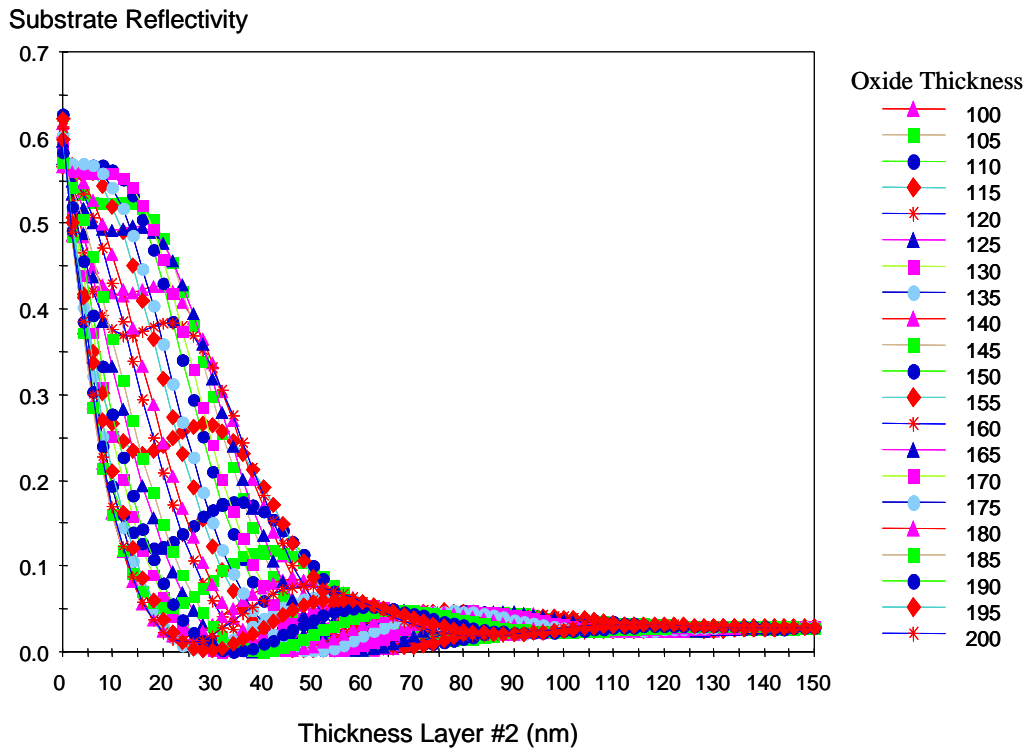


Figure 5. Substrate reflectivity versus BARC thickness over a range of underlying oxide thicknesses (oxide on top of a silicon substrate).

The second type of BARC optimization problem involves the use of a BARC on a transparent substrate, such as an oxide film. For such a case, the overall substrate reflectivity will be a function of the oxide thickness and one of the goals of the BARC design is to reduce the sensitivity to underlying film thickness variations. As can be seen from Figure 5, using the BARC at a first minimum results in a very large sensitivity to underlying oxide thickness variations. In fact, the thickest BARC films provide the most robust behavior. Thus, the preferred design approach for this case is to determine the maximum allowed BARC thickness from an integration perspective, then optimize the n & k values of the BARC to minimize reflectivity over the range of expected oxide thicknesses.

How critical is BARC optimization? How low must the substrate reflectivity be before acceptable CD control can be expected? At what level of substrate reflectivity can I ignore swing curves and choosing the optimum resist thickness? There is no single answer to these questions, since they are process and feature dependent. But consider the example shown in Figure 6. Here, 100nm lines with a 280nm pitch are simulated with a stepper using annular illumination, with a center sigma given by $\sigma_{NA} = 0.54$. As can be seen, a substrate reflectivity of less than 0.1% still leads to a noticeable swing behavior.

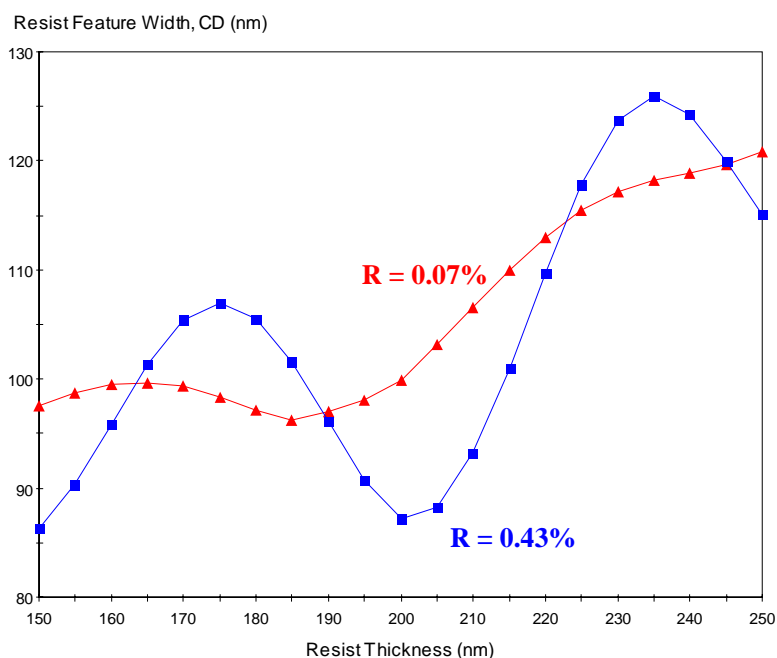


Figure 6. CD swing curves (100nm lines with a 280nm pitch are printed with a stepper using annular illumination, with a center sigma given by $\sigma_{NA} = 0.54$) for two different BARCs with different levels of optimization, as given by the resulting substrate reflectivity R .

B. Process Window Prediction

The effect of focus on a projection lithography system (such as a stepper) is a critical part of understanding and controlling a lithographic process. This section will address the importance of focus by providing definitions of the *process window* and *depth of focus* (DOF). Simulation proves an invaluable tool for predicting focus effects, generating process windows, and determining realistic values for the DOF. In a manufacturing environment, being able to predict the size of the process window for many different

processes and features enables the process engineer to determine which process layers are likely to be problematic given the known sources of focus and exposure errors in the fab, and which critical features to track and how closely.

In general, DOF can be thought of as the range of focus errors that a process can tolerate and still give acceptable lithographic results. Of course, the key to a good definition of DOF is in defining what is meant by tolerable. A change in focus results in two major changes to the final lithographic result: the photoresist profile changes and the sensitivity of the process to other processing errors is increased. Typically, photoresist profiles are described using three parameters: the linewidth (or critical dimension, CD), the sidewall angle, and the final resist thickness. The variation of these parameters with focus can be readily determined for any given set of conditions. The second effect of defocus is significantly harder to quantify: as an image goes out of focus, the process becomes more sensitive to other processing errors such as exposure dose and develop time. Of these secondary process errors, the most important is exposure.

Since the effect of focus is dependent on exposure, the only way to judge the response of the process to focus is to simultaneously vary both focus and exposure in what is known as a *focus-exposure matrix*. Figure 7 shows a typical example of the output of a focus-exposure matrix using linewidth as the response (sidewall angle and resist loss can also be plotted in the same way) in what is called a Bossung plot. Of course, one output as a function of two inputs can be plotted in several different ways. For example, the Bossung curves could also be plotted as exposure latitude curves (linewidth versus exposure) for different focus settings. Probably the most useful way to plot this two-dimensional data set is a contour plot – contours of constant linewidth versus focus and exposure (Figure 8).

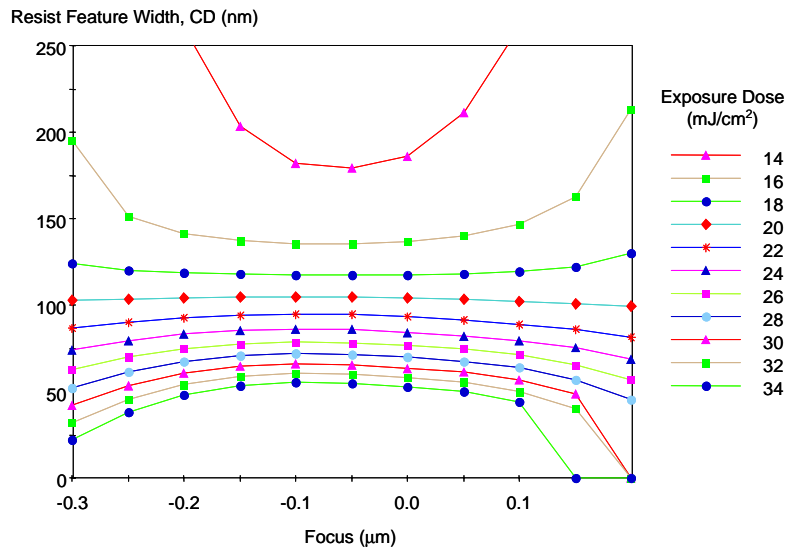


Figure 7. Example of the effect of focus and exposure on the resulting resist linewidth. Focal position is defined as zero at the top of the resist with a negative focal position indicating that the plane of focus is inside the resist.

The contour plot form of data visualization is especially useful for establishing the limits of exposure and focus that allow the final image to meet certain specifications. Rather than plotting all of the contours of constant CD, one could plot only the two CDs corresponding to the outer limits of acceptability – the CD specifications. Because of the nature of a contour plot, other variables can also be plotted on the

same graph. Figure 9 shows an example of plotting contours of CD (nominal $\pm 10\%$), 80° sidewall angle, and 10% resist loss all on the same graph. The result is a *process window* – the region of focus and exposure that keeps the final resist profile within all three specifications.

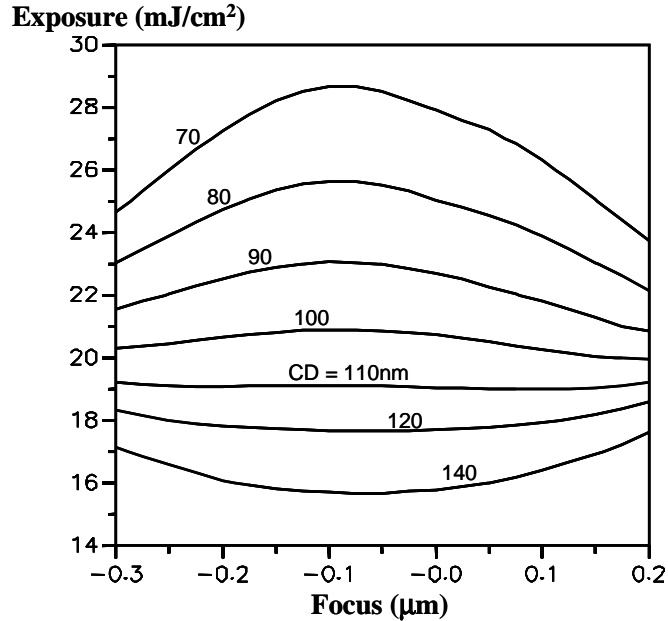


Figure 8. Displaying the data from a focus-exposure matrix in an alternate form, contours of constant CD versus focus and exposure.

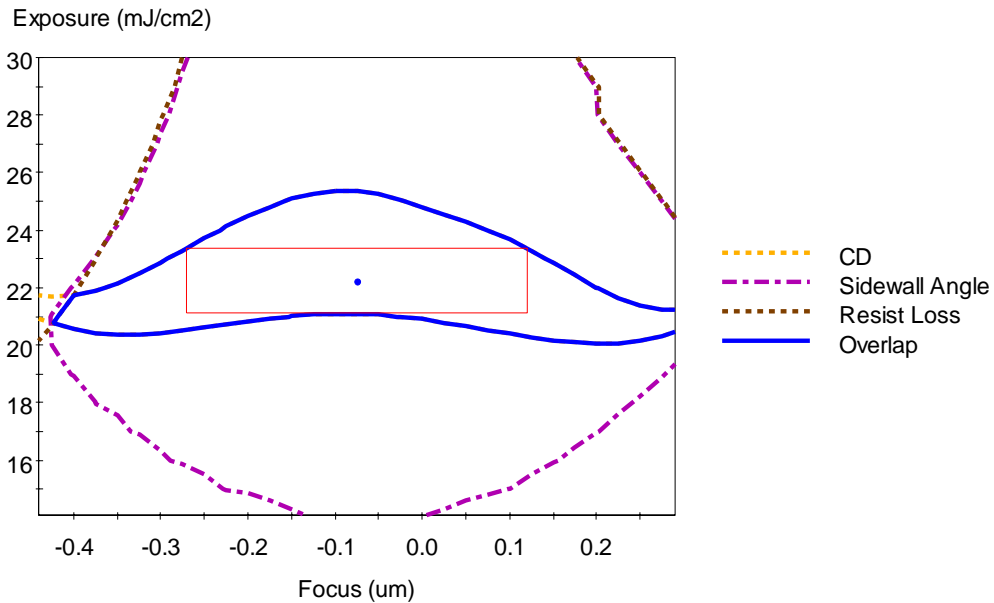


Figure 9. The focus-exposure process window is constructed from contours of the specifications for linewidth, sidewall angle, and resist loss. The shaded area shows the overall process window.

The focus-exposure process window is one of the most important plots in lithography since it shows how exposure and focus work together to affect linewidth, sidewall angle, and resist loss. The process window can be thought of as a *process capability* – how the process responds to changes in focus and exposure. How can we determine if a given process capability is good enough? An analysis of the error sources for focus and exposure in a given process will give a *process requirement*. If the process capability exceeds the process requirements, yield will be high. If, however, the process requirement is too large to fit inside the process capability, yield will suffer. A thorough analysis of the effects of exposure and focus on yield can be accomplished with yield modeling (to be discussed in a later section), but a simpler analysis can give useful insight and can be used to derive a number for depth of focus.

What is the maximum range of focus and exposure (that is, the maximum process requirement) that can fit inside the process window? A simple way to investigate this question is to graphically represent errors in focus and exposure as a rectangle on the same plot as the process window. The width of the rectangle represents the built-in focus errors of the processes, and the height represents the built-in dose errors. The problem then becomes one of finding the maximum rectangle that fits inside the process window. However, there is no one answer to this question. There are many possible rectangles of different widths and heights that are “maximum”, i.e., they cannot be made larger in either direction without extending beyond the process window. (Note that the concept of a “maximum area” is meaningless here.) Each maximum rectangle represents one possible trade-off between tolerance to focus errors and tolerance to exposure errors. Larger DOF can be obtained if exposure errors are minimized. Likewise, exposure latitude can be improved if focus errors are small. The result is a very important trade-off between exposure latitude and DOF.

If all focus and exposure errors were systematic, then the proper graphical representation of those errors would be a rectangle. The width and height would represent the total ranges of the respective errors. If, however, the errors were randomly distributed, then a probability distribution function would be needed to describe them. For the completely random case, a Gaussian distribution with standard deviations in exposure and focus is used to describe the probability of a given error. In order to graphically represent the errors of focus and exposure, one should describe a surface of constant probability of occurrence. All errors in focus and exposure inside the surface would have a probability of occurring that is greater than the established cutoff. What is the shape of such a surface? For fixed systematic errors, the shape is a rectangle. For a Gaussian distribution, the surface is an ellipse. If one wishes to describe a “three-sigma” surface, the result would be an ellipse with major and minor axes equal to the three-sigma errors in focus and exposure.

Using either a rectangle for systematic errors or an ellipse for random errors, the size of the errors that can be tolerated for a given process window can be determined. Taking the rectangle as an example, one can find the maximum rectangle that will fit inside the processes window. Figure 10 shows an analysis of the process window where every maximum rectangle is determined and its height (the exposure latitude) plotted versus its width (depth of focus). Likewise, assuming random errors in focus and exposure, every maximum ellipse that fits inside the processes window can be determined. The horizontal width of the ellipse would represent a three-sigma error in focus, while the vertical height of the ellipse would give a three-sigma error in exposure. Plotting the height versus the width of all the maximum ellipses gives the second curve of exposure latitude versus DOF in Figure 10.

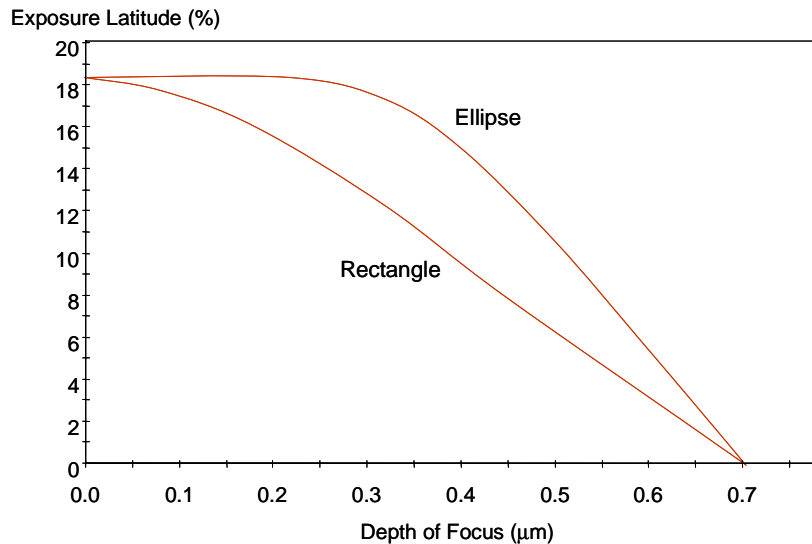


Figure 10. The process window of Figure 9 is analyzed by fitting all the maximum rectangles and all the maximum ellipses, then plotting their height (exposure latitude) versus their width (depth of focus).

The exposure latitude versus DOF curves of Figure 10 provide the most concise representation of the coupled effects of focus and exposure on the lithography process. Each point on the exposure latitude - DOF curve is one possible operating point for the process. The user must decide how to balance the trade-off between DOF and exposure latitude. One approach is to define a minimum acceptable exposure latitude, and then operate at this point; this has the effect of maximizing the DOF of the process. In fact, this approach allows for the definition of a single value for the DOF of a given feature for a given process. The depth of focus of a feature can be defined as *the range of focus that keeps the resist profile of a given feature within all specifications (linewidth, sidewall angle, and resist loss) over a specified exposure range*. For the example given in Figure 10, a minimum acceptable exposure latitude of 15%, in addition to the other profile specifications, would lead to the following depth of focus results:

$$\begin{aligned} \text{DOF (rectangle)} &= 0.40 \mu\text{m} \\ \text{DOF (ellipse)} &= 0.52 \mu\text{m} \end{aligned}$$

As one might expect, systematic errors in focus and exposure are more problematic than random errors, leading to a smaller DOF. Most actual processes would have a combination of systematic and random errors. Thus, one might expect the rectangle analysis to give a pessimistic value for the DOF, and the ellipse method to give an optimistic view of DOF. The average value of the two will be a more realistic number in most cases.

The definition of depth of focus also leads naturally to the determination of best focus and best exposure. The DOF value read off from the exposure latitude versus DOF curve corresponds to one maximum rectangle or ellipse that fit inside the process window. The center of this rectangle or ellipse would then correspond to best focus and exposure for this desired operating point.

Although all of the above results describe the focus and exposure response of one critical feature, in reality a number of mask features must be printed simultaneously. Using the most common example,

isolated lines typically occur on the same design as dense lines. Thus, a more important measure of performance than the DOF of each individual feature is the overlapping DOF of both features. Just as multiple profile metrics were overlapped to form one overlapping process window in Figure 9, process windows from different features can be overlapped to determine the DOF for simultaneously printing those multiple features. Figure 11 shows such an example for isolated and dense features.

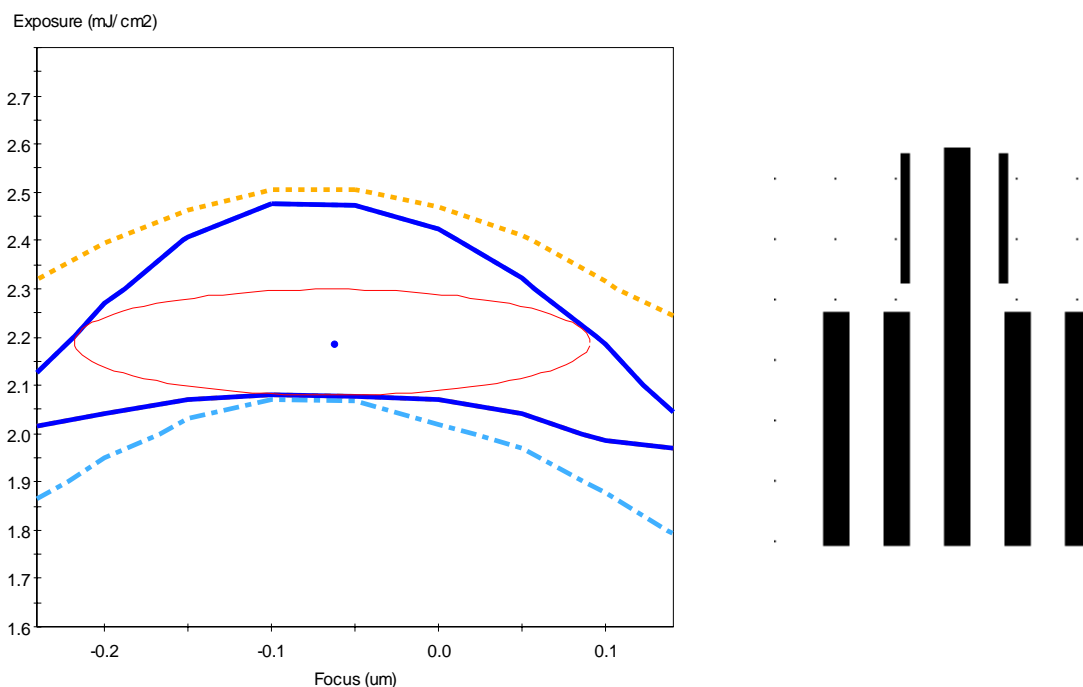


Figure 11. The overlapping process window for the dense and isolated features shown to the right of the graph.

All of the above graphs were generated using simulation, which can not only generate focus-exposure data, but can analyze the data to determine the process window and DOF as well. Overlapping process windows were calculated using multiple metrology planes for a given simulation.

C. NA/σ optimization

At the time of process development, the numerical aperture and illumination shape of the stepper/scanner are optimized by maximizing the overlapping process window of the critical features of a design. However, once the numerical aperture and illumination shape have been set for a process, they are not readily changed. This is because of the strong dependence of the OPC models on the optical settings of the exposure tool. Once the OPC has been applied to a design and a mask has been made, that mask is unlikely to function well on a tool with different NA or partial coherence (σ) settings. However, there are still some circumstances when NA/σ optimization is needed in a manufacturing environment based on an inevitable truth: things change. Since the time when the OPC was applied and the mask made, circumstances in the fab can change. For example,

- A new, higher numerical aperture stepper is now available in the fab. Would the existing product yield higher on this new stepper? If so, what NA/illumination is optimum?
- There is a need for cost reduction on a product whose sales price is declining quickly. Can the same mask be used on an older stepper (possibly one with more aberrations or flare) in order to lower cost?
- Why does a given mask produce better results on stepper A versus stepper B?
- Can we predict ahead of time what the best dose will be for a new mask, given the right mask measurements?
- A set process is being transferred from one fab to another, but the scanners are not identical. How can I set up the parameters of the new scanner to best match the scanner on which the process was developed?

D. OPC Verification

Ideally, OPC models, calibrated to a given fab process, produce corrected mask designs that will give good yield due to good CD control and no catastrophic lithography failures. Life is not always so predictable. For a wide range of reasons, The final OPC-complete design may have errors that show up consistently or intermittently in the fab, usually without warning. Using simulation to independently verify the output of OPC tools is becoming more and more common today.

E. CD Limited Yield, Cpk Analysis

A result of the tighter specifications of new generations of device technologies is the increased need to understand and control the CD distribution of lithography processes. Better control of the CD distribution will lead to higher yields and more favorable bin sorting of the final product. To predict the CD distribution and associated statistical metrics such as mean, standard deviation, Cpk, and the parametric CD yield of a photolithographic process using simulation, a simple three step process is used, as shown in Figure 12 [44-47]. First, an analysis of a lithographic process must be performed to determine the error distributions of the input parameters. For example, it may be determined that exposure varies in a normal distribution with a mean at the nominal setting and a standard deviation of 5%. Second, PROLITH is used to create a multi-variable process response space (for example, final resist critical dimension (CD) versus focus, exposure, resist thickness, etc.). The range of each input variable is chosen to completely cover the range of possible set points plus their errors (usually over a $\pm 3\sigma$ range). Third, by correlating the input error distribution with the process response space, a final CD distribution is generated. Analysis of the output distribution produces a predicted parametric CD yield using some acceptance criterion for CD and a calculated value for Cpk, as well as the more common mean and standard deviation. These numbers can be used to help optimize the performance of a given process.

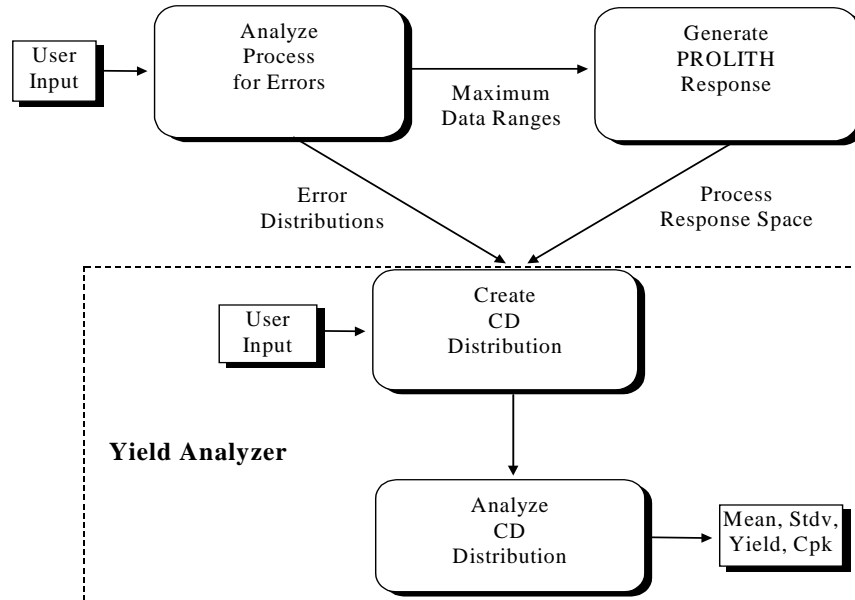


Figure 12. Methodology for using PROLITH with the Yield Analyzer to predict and analyze CD distributions.

Consider a simple example to illustrate the method -- the effect of exposure errors on linewidth. The process response in this case is the well known exposure latitude curve. If the input error distribution is known, correlation of the input error probability with the process response function gives the output error distribution. For this example let us assume that the exposure errors are normally distributed about the mean with a 3σ of 10% (Figure 13).

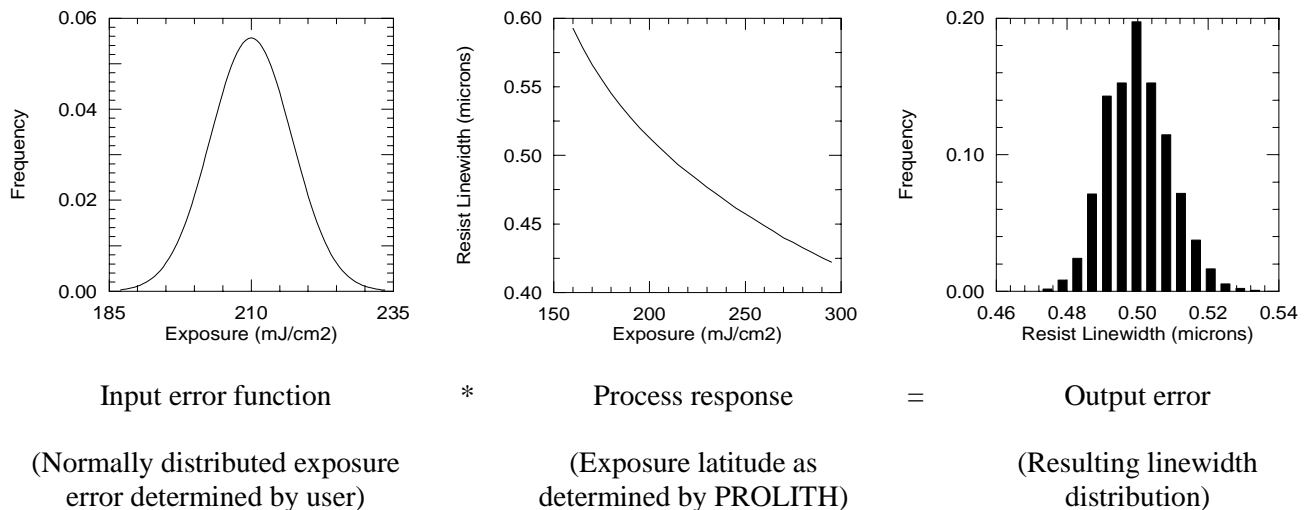


Figure 13. Resulting error distribution from a one-dimensional process response.

The error distribution is plotted as the frequency of occurrence (or probability of occurrence) versus exposure energy with arbitrary units for frequency. The process response is linewidth versus exposure energy as predicted using simulation. For any given exposure energy, there is a probability that this energy

will occur (for example, 200 mJ/cm² has a probability of 0.021 in Figure 13). From the process response curve, an exposure energy corresponds to a specific CD (for example, 0.513 μm for an energy of 200 mJ/cm²) and thus must have the probability of occurrence corresponding to the probability of the exposure energy. Correlation of the input error distribution with the process response results in a list of linewidth values with corresponding frequencies of occurrence. The linewidth can then be divided up into equal size bins (for Figure 13, the bin size is 0.004 μm) and all of the probabilities with CDs within a given bin are summed. The result is plotted as a histogram of frequency versus CD and represents the resulting output CD error distribution.

The power of the CD distribution method is its ability to investigate CD errors in the presence of multiple error sources, and to optimize the process for the most important metric in lithography: CD distribution. Many types of investigations are possible, including examining the effects of focus and exposure errors on CD distributions, determining of the optimum numerical aperture and partial coherence of a stepper, evaluation of the impact of process improvements on CD yield, influence of film stack variations on the distribution of reflectivities, and thousands of other possibilities. The result of many of these investigations show that the optimum process settings, taking into account process errors inherent in a manufacturing environment, are substantially different than the optimums determined by using other methodologies. This behavior is a result of the highly non-linear nature of lithography and underscores the benefits of using simulation coupled with statistical analysis.

F. Troubleshooting/Root Cause Analysis

Once simulation is in common usage in a manufacturing environment, principally to serve use cases such as those described above, another important application of simulation will inevitably surface: troubleshooting. The scenario is common one: something has gone wrong (the CD distribution has widened, or the resist profile is exhibiting some anomaly such as a foot), but the cause is unknown. Various theories are proposed as to the root cause (the resist foot is caused by an optical interference effect, or by a chemical interaction with the BARC, for example). Experiments are devised that could help choose between the competing theories. In many cases, simulation can be used to carry out or refine these experiments. For the example of the resist footing problem, are there any potential film stack variations that could cause this effect? If so, make some measurements to confirm this scenario. If not, look for another cause. As the litho engineers in the fab become more comfortable with the usefulness and accuracy of simulation (including an understanding of its limitations), its use in troubleshooting will become increasingly common.

3. CONCLUSIONS

Optical lithography simulation has become an indispensable tool for research, development and manufacturing. There are four major uses for lithography simulation: 1) as a research tool, 2) as a development and process optimization tool, 3) as a manufacturing tool, and 4) as a learning tool, to help provide a fundamental understanding of all aspects of the lithography process. In this paper, numerous examples of the use of simulation as a manufacturing tool have been given. The most common use cases for lithography simulation in a manufacturing environment are:

- Film Stack Optimization
- Process Window Prediction
- NA/σ optimization
- OPC Verification
- CD Limited Yield, Cpk Analysis

- Troubleshooting/Root Cause Analysis

Other use cases are currently being investigated by many users of lithography simulation and will undoubtedly lead to even greater use of lithography simulation in manufacturing environments.

4. REFERENCES

1. A. R. Neureuther and F. H. Dill, "Photoresist Modeling and Device Fabrication Applications," Optical And Acoustical Micro-Electronics, Polytechnic Press (New York: 1974) pp. 233-249.
2. H. L. Stover, M. Nagler, I. Bol, and V. Miller, "Submicron Optical Lithography: I-line Lens and Photoresist Technology," *Optical Microlith. III*, Proc., SPIE Vol. 470 (1984) pp. 22-33.
3. I. I. Bol, "High-Resolution Optical Lithography using Dyed Single-Layer Resist," *Kodak Microelec. Seminar Interface '84* (1984) pp. 19-22.
4. M. D. Levenson, N. S. Viswanathan, R. A. Simpson, "Improving Resolution in Photolithography with a Phase-Shifting Mask," *IEEE Trans. Electron Devices*, Vol. ED-29, No. 12 (Dec. 1982) pp. 1828-1836.
5. M. D. Levenson, D. S. Goodman, S. Lindsey, P. W. Bayer, and H. A. E. Santini, "The Phase-Shifting Mask II: Imaging Simulations and Submicrometer Resist Exposures," *IEEE Trans. Electron Devices*, Vol. ED-31, No. 6 (June 1984) pp. 753-763.
6. M. D. Prouty and A. R. Neureuther, "Optical Imaging with Phase Shift Masks," *Optical Microlith. III*, Proc., SPIE Vol. 470 (1984) pp. 228-232.
7. C. A. Mack, "Optimum Stepper Performance Through Image Manipulation," *KTI Micro-electronics Seminar, Proc.*, (1989) pp. 209-215.
8. C. A. Mack, "Algorithm for Optimizing Stepper Performance Through Image Manipulation," *Optical/Laser Microlithography III, Proc.*, SPIE Vol. 1264 (1990) pp. 71-82.
9. H. Fukuda, T. Terasawa, and S. Okazaki, "Spatial Filtering for Depth-of-focus and Resolution Enhancement in Optical Lithography," *Journal of Vacuum Science and Technology*, Vol. B9, No. 6 (Nov/Dec 1991) pp. 3113-3116.
10. C. A. Mack and J. E. Connors, "Fundamental Differences Between Positive and Negative Tone Imaging," *Optical/Laser Microlithography V, Proc.*, SPIE Vol. 1674 (1992) pp. 328-338, and *Microlithography World*, Vol. 1, No. 3 (Jul/Aug 1992) pp. 17-22.
11. C. A. Mack, "Lithographic Optimization Using Photoresist Contrast," *KTI Microlithography Seminar, Proc.*, (1990) pp. 1-12, and *Microelectronics Manufacturing Technology*, Vol. 14, No. 1 (Jan. 1991) pp. 36-42.
12. C. A. Mack, "Photoresist Process Optimization," *KTI Microelectronics Seminar, Proc.*, (1987) pp. 153-167.
13. P. Trefonas and C. A. Mack, "Exposure Dose Optimization for a Positive Resist Containing Poly-functional Photoactive Compound," *Advances in Resist Technology and Processing VIII, Proc.*, SPIE Vol. 1466 (1991).
14. J. S. Petersen, C. A. Mack, J. Sturtevant, J. D. Byers and D. A. Miller, "Non-constant Diffusion Coefficients: Short Description of Modeling and Comparison to Experimental Results," *Advances in Resist Technology and Processing XII, Proc.*, SPIE Vol. 2438 (1995).
15. C. A. Mack and P. M. Kaufman, "Mask Bias in Submicron Optical Lithography," *Jour. Vac. Sci. Tech.*, Vol. B6, No. 6 (Nov./Dec. 1988) pp. 2213-2220.
16. N. Shamma, F. Sporon-Fielder and E. Lin, "A Method for Correction of Proximity Effect in Optical Projection Lithography," *KTI Microelectronics Seminar, Proc.*, (1991) pp. 145-156.
17. A. R. Neureuther, P. Flanner III, and S. Shen, "Coherence of Defect Interactions with Features in Optical Imaging," *Jour. Vac. Sci. Tech.*, Vol. B5, No. 1 (Jan./Feb. 1987) pp. 308-312.

18. J. Wiley, "Effect of Stepper Resolution on the Printability of Submicron 5x Reticle Defects," *Optical/Laser Microlithography II, Proc.*, SPIE Vol. 1088 (1989) pp. 58-73.
19. L.M. Milner, K.C. Hickman, S.M. Gasper, K.P. Bishop, S.S.H. Naqvi, J.R. McNeil, M. Blain, and B.L. Draper, "Latent Image Exposure Monitor Using Scatterometry," SPIE Vol. 1673 (1992) pp. 274-283.
20. K.P. Bishop, L.M. Milner, S.S.H. Naqvi, J.R. McNeil, and B.L. Draper, "Use of Scatterometry for Resist Process Control," SPIE Vol. 1673 (1992) pp. 441-452
21. L.M. Milner, K.P. Bishop, S.S.H. Naqvi, and J.R. McNeil, "Lithography Process Monitor Using Light Diffracted from a Latent Image," SPIE Vol. 1926 (1993) pp. 94-105.
22. S. Zaidi, S.L. Prins, J.R. McNeil, and S.S.H. Naqvi, "Metrology Sensors for Advanced Resists," SPIE Vol. 2196 (1994) pp. 341-351
23. J.R. Johnson, G.J. Stagaman, J.C. Sardella, C.R. Spinner III, F. Liou, P. Tiefonas, and C. Meister, "The Effects of Absorptive Dye Loading and Substrate Reflectivity on a 0.5 μm I-line Photoresist Process," SPIE Vol. 1925 (1993) pp. 552-563.
24. W. Conley, R. Akkapeddi, J. Fahey, G. Hefferon, S. Holmes, G. Spinillo, J. Turtevant, and K. Welsh, "Improved Reflectivity Control of APEX-E Positive Tone Deep-UV Photoresist," SPIE Vol. 2195 (1994) pp. 461-476.
25. N. Thane, C. Mack, and S. Sethi, "Lithographic Effects of Metal Reflectivity Variations," SPIE Vol. 1926 (1993) pp. 483-494.
26. B. Singh, S. Ramaswami, W. Lin, and N. Avadhany, "IC Wafer Reflectivity Measurement in the UV and DUV and Its Application for ARC Characterization," SPIE Vol. 1926 (1993) pp. 151-163.
27. S.S. Miura, C.F. Lyons, and T.A. Brunner, "Reduction of Linewidth Variation over Reflective Topography," SPIE Vol. 1674 (1992) pp. 147-156.
28. H. Yoshino, T. Ohfuji, and N. Aizaki, "Process Window Analysis of the ARC and TAR Systems for Quarter Micron Optical Lithography," SPIE Vol. 2195 (1994) pp. 236-245.
29. G. Flores, W. Flack, and L. Dwyer, "Lithographic Performance of a New Generation I-line Optical System: A Comparative Analysis," SPIE Vol. 1927 (1993) pp. 899-913.
30. B. Kuyel, M. Barrick, A. Hong, and J. Vigil, "0.5 Micron Deep UV Lithography Using a Micrascan-90 Step-And-Scan Exposure Tool," SPIE Vol. 1463 (1991) pp. 646-665.
31. G.E. Flores, W.W. Flack, and E. Tai, "An Investigation of the Properties of Thick Photoresist Films," SPIE Vol. 2195 (1994) pp. 734-751.
32. H. Iwasaki, T. Itani, M. Fujimoto, and K. Kasama, "Acid Size Effect of Chemically Amplified Negative Resist on Lithographic Performance," SPIE Vol. 2195 (1994) pp. 164-172.
33. U. Schaedeli, N. Münzel, H. Holzwarth, S.G. Slater, and O. Nalamasu, "Relationship Between Physical Properties and Lithographic Behavior in a High Resolution Positive Tone Deep-UV Resist," SPIE Vol. 2195 (1994) pp. 98-110.
34. K. Schlicht, P. Scialdone, P. Spragg, S.G. Hansen, R.J. Hurditch, M.A. Toukhy, and D.J. Brzozowy, "Reliability of Photospeed and Related Measures of Resist Performances," SPIE Vol. 2195 (1994) pp. 624-639.
35. R.A. Cirelli, E.L. Raab, R.L. Kostelak, and S. Vaidya, "Optimizing Numerical Aperture and Partial Coherence to Reduce Proximity Effect in Deep-UV Lithography," SPIE Vol. 2197 (1994) pp. 429-439.
36. B. Katz, T. Rogoff, J. Foster, B. Rericha, B. Rolfson, R. Holscher, C. Sager, and P. Reynolds, "Lithographic Performance at Sub-300 nm Design Rules Using High NA I-line Stepper with Optimized NA and σ in Conjunction with Advanced PSM Technology," SPIE Vol. 2197 (1994) pp. 421-428.
37. P. Luehrmann, and S. Wittekoek, "Practical 0.35 μm I-line Lithography," SPIE Vol. 2197 (1994) pp. 412-420.
38. V.A. Deshpande, K.L. Holland, and A. Hong, "Isolated-grouped Linewidth Bias on SVGL Micrascan," SPIE Vol. 1927 (1993) pp. 333-352.

39. R.C. Henderson, and O.W. Otto, "Correcting for Proximity Effect Widens Process Latitude," SPIE Vol. 2197 (1994) pp. 361-370.
40. H. Engstrom and J. Beacham, "Online Photolithography Modeling Using Spectrophotometry and PROLITH/2," SPIE Vol. 2196 (1994) pp. 479-485.
41. J. Kasahara, M. V. Dusa, and T. Perera, "Evaluation of a Photoresist Process for 0.75 Micron, G-line Lithography," SPIE Vol. 1463 (1991) pp. 492-503.
42. E. A. Puttlitz, J. P. Collins, T. M. Glynn, L. L. Linehan, "Characterization of Profile Dependency on Nitride Substrate Thickness for a Chemically Amplified I-line Negative Resist," SPIE Vol. 2438 (1995) pp. 571-582.
43. P. M. Mahoney and C. A. Mack, "Cost Analysis of Lithographic Characterization: An Overview," *Optical/Laser Microlithography VI, Proc.*, SPIE Vol. 1927 (1993) pp. 827-832.
44. C.A. Mack and E.W. Charrier, "Yield Modeling for Photolithography", OCG Interface '94 (1994), pp. 171-182.
45. E.W. Charrier and C.A. Mack, "Yield Modeling and Enhancement for Optical Lithography," *Optical/Laser Microlithography VIII, Proc.*, SPIE Vol. 2440 (1995), pp 435-447.
46. E. W. Charrier, C.J. Progler, C.A. Mack, "Comparison of Simulated and Experimental CD-Limited Yield for a Submicron i-Line Process", *Microelectronic Manufacturing, Yield, Reliability and Failure Analysis*, Proc. SPIE Vol 2635, (1995), pp. 84-94.
47. E.W. Charrier, C.A. Mack, Q. Zuo, M. Maslow, "Methodology for Utilizing CD Distributions for Optimization of Lithographic Processes," *Optical Microlithography X, Proc.*, SPIE (1997).